

RESEARCH ARTICLE

10.1002/2015SW001351

Key Points:

- COSMIC retrieval accuracy of electron density depends on time season and latitude
- Latitudinal distribution of deviation in COSMIC profiles shows a maximum at EIA
- Error in COSMIC measurements increases significantly during magnetic storms

Correspondence to:

D. Siingh,
devendraasiingh@tropmet.res.in;
devendraasiingh@gmail.com

Citation:

Kumar, S., R. P. Singh, E. L. Tan, A. K. Singh, R. N. Ghodpage, and D. Siingh (2016), Temporal and spatial deviation in F_2 peak parameters derived from FORMOSAT-3/COSMIC, *Space Weather*, 14, doi:10.1002/2015SW001351.

Received 18 DEC 2015

Accepted 14 MAY 2016

Accepted article online 18 MAY 2016

Temporal and spatial deviation in F_2 peak parameters derived from FORMOSAT-3/COSMIC

Sanjay Kumar^{1,2}, R. P. Singh¹, Eng Leong Tan², A. K. Singh¹, R. N. Ghodpage³, and Devendra Siingh⁴

¹Department of Physics, Banaras Hindu University, Varanasi, India, ²School of Electrical and Electronic Engineering, Nanyang Technological University, Singapore, ³Indian Institute of Geomagnetism, Shivaji University Campus, Kolhapur, India, ⁴Indian Institute of Tropical Meteorology, Pune, India

Abstract The plasma frequency profiles derived from the Constellation of Observing System for Meteorology, Ionosphere and Climate (COSMIC) radio occultation measurements are compared with ground-based ionosonde data during the year 2013. Equatorial and midlatitude five stations located in the Northern and Southern Hemisphere are considered: Jicamarca, Jeju, Darwin, Learmonth, and Juliusruh. The aim is to validate the COSMIC-derived data with ground-based measurements and to estimate the difference in plasma frequency (which represents electron density) and height of F_2 layer peak during the daytime/nighttime and during different seasons by comparing the two data sets. Analysis showed that the nighttime data are better correlated than the daytime, and the maximum difference occurs at the equatorial ionospheric anomaly (EIA) station as compared to lower and midlatitude stations during the equinox months. The difference between daytime and nighttime correlations becomes insignificant at midlatitude stations. The statistical analysis of computed errors in f_oF_2 (h_mF_2) showed Gaussian nature with the most probable error range of $\pm 15\%$ ($\pm 10\%$) at the equatorial and EIA stations, $\pm 9\%$ ($\pm 7\%$) outside the EIA region which reduced to $\pm 8\%$ ($\pm 6\%$) at midlatitude stations. The reduction in error at midlatitudes is attributed to the decrease in latitudinal electron density gradients. Comparing the analyzed data during the three geomagnetic storms and quiet days of the same months, it is observed that the differences are significantly enhanced during storm periods and the magnitude of difference in f_oF_2 increases with the intensity of geomagnetic storm.

1. Introduction

Electron density profiles play important roles in the study of ionospheric storm, ion compositions, plasma temperature, radio communications between satellite and ground receivers, and other ionospheric-dynamic phenomena [Lei et al., 2007; Kelley et al., 2009; Chu et al., 2009]. The transition region from photochemical dominance to diffusion dominance called F_2 region is described by peak density (N_mF_2) and height of the F_2 layer (h_mF_2), which has been the most focused area. F_2 region and its dynamics have been studied from a constellation of six microsatellites, termed as the Formosa Satellite Mission (FORMOSAT)-3/Constellation of Observing System for Meteorology, Ionosphere and Climate (COSMIC) [He et al., 2009; Tsai et al., 2009; Liu et al., 2009, 2010, 2011; Aragon-Angel et al., 2011; Ely et al., 2012; Zakharenkova et al., 2012; Yue et al., 2012, 2014; Chuo et al., 2013; Hu et al., 2014]. COSMIC radio occultation (RO) data have been widely used to monitor ionospheric variability, ionospheric weather (geomagnetic storm response, solar flare response, lower atmospheric driving disturbances), climate change simulation and validation, etc [Kirchengast et al., 2004; Lei et al., 2007; Liou et al., 2010; Krankowski et al., 2011; Yue et al., 2012, 2104; Kumar et al., 2014]. Each microsatellite has a tiny ionospheric photometer to observe the nighttime ionospheric airglow OI 135.6 nm emission and a triband beacon to obtain atmospheric and ionospheric information through recording the phase and Doppler shifts of GPS signals [Rocken et al., 2000; Cheng et al., 2006; Ghodpage et al., 2012]. The GPS occultation payloads on six microsatellites can provide up to 2500 vertical ionospheric electron density profiles every day [Hu et al., 2014] from the measured L_1 and L_2 phase path difference [Hajj and Romans, 1998; Lei et al., 2007]. GPS L band signals are also sensitive to ionospheric density irregularities along the ray path, and hence, sharp sporadic E layer and F region irregularities can also be characterized.

In the retrieval of electron density profile from the COSMIC GPS occultation data, Abel inversion is used with several assumptions/approximations such as (i) straight line signal propagation, (ii) spherical symmetry of electron density profiles, (iii) circular satellite orbits, and (iv) first-order estimation of the electron density at the top [Kuo et al., 2004; Syndergaard et al., 2006]. Among all the assumptions, the assumption of spherical symmetry in the horizontal direction is the most significant source of error [Tsai et al., 2001; Tsai and Tsai, 2004; Liu et al., 2010; Yue et al., 2010; Kumar

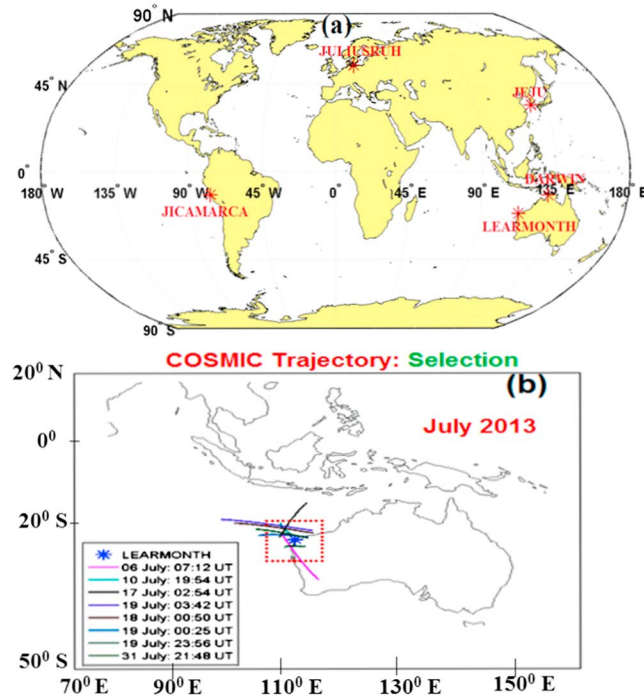


Figure 1. (a) Map showing the geographical location of ionosonde stations involved in this study (b) The ionosonde location at Learmonth and the region of COSMIC observations. The blue asterisk symbol denotes ionosonde at Learmonth (21.8°S, 114.10°E), Australia, while the 10° × 10° square are the selection region of the COSMIC trajectory tangent points.

et al., 2014]. The electron density is derived based on the physical principle that refractivity is proportional to electron density in an ionized medium [Parkinson and Spilker, 1996]. Yue *et al.* [2010] reported that the reliability of the retrieved electron density profile is lower at low altitudes in low-latitude regions and that the errors were caused by the horizontal inhomogeneities of electron density. Comparison of N_mF_2 and h_mF_2 ionospheric parameters at the equatorial latitude [Chu *et al.*, 2010] and low latitudes [Straus, 2007; Wu *et al.*, 2009] indicated that the accuracy of RO measurements were better in N_mF_2 than h_mF_2 . The discrepancy between them is smaller in low- and middle-latitude regions and larger in high-latitude regions [Chu *et al.*, 2010]. Hu *et al.* [2014] reported that the correlation between COSMIC and ionosonde measurements decreased at high solar activity, and the correlation of N_mF_2 was higher during the nighttime, while correlation of h_mF_2 was higher during the daytime.

In spite of a number of works comparing the COSMIC RO measurements with ground-based measurements (ionosonde and incoherent scatter radar) [Lei *et al.*, 2007; Tsai *et al.*, 2009; Aragon-Angel *et al.*, 2011; Hu *et al.*, 2014; Yue *et al.*, 2014] almost no work (to the best of authors' knowledge) related with the validation of COSMIC RO measurements with ground-based measurements during space weather events (solar flares, geomagnetic storms, etc) is available. In this paper, we examine the variations in difference (error) of COSMIC-derived plasma frequency (f_oF_2) and altitude of F_2 peak (h_mF_2) from ionosonde data at five different latitudes: near equator, Jicamarca (geographical latitude 12.0°S, longitude 76.8°W, geomagnetic latitude 2.15° N), in low-latitude region, Jeju (geographical latitude 33.8°N, longitude 126.10°E, geomagnetic latitude 23.92° N), equatorial ionospheric anomaly (EIA) region, Darwin (geographical latitude 12.5°S, longitude 130.9°E, geomagnetic latitude 21.3°S), near the edge of EIA region, Learmonth (geographical latitude 21.8°S, longitude 114.10°E, geomagnetic latitude 31.41°S), and the midlatitude region, Juliusruh (geographical latitude 54.6°N, longitude 13.4°E, geomagnetic latitude 53.96°N). The location of the stations is shown in Figure 1a. We have also studied the impact of geomagnetic storm on the magnitude of differences (errors) in COSMIC data by analyzing the data during quiet period and geomagnetic storm period. Data sources and analysis are given in section 2. Results are discussed in section 3, which is followed by the conclusion section 4.

2. Data Sources and Analysis

The ionospheric F layer peak plasma frequency parameter f_oF_2 and peak height parameter h_mF_2 were retrieved from both satellite and ionosonde measurements for the year 2013. In the present analysis COSMIC RO data are obtained from the COSMIC Data Analysis and Archive Center at the University Corporation for Atmospheric Research (UCAR) from the website (<http://cdaac-www.cosmic.ucar.edu>). The site of an occultation event is considered to be the location of the tangential point at the F_2 peak height h_mF_2 [Jakowski *et al.*, 2002]. Therefore, in order to validate the COSMIC profile with ionosonde profile, we have selected only those trajectories whose tangent point at F_2 peak altitude lied within $\pm 5^\circ$ of the ionosonde location and passing around at the same time (± 5 min) of ionosonde measurements. The COSMIC trajectory

selection criterion for Learmonth, Australia, is shown in Figure 1b and is marked by asterisk with blue color, and the area of the COSMIC trajectory is marked by the square with red color. The ionosonde routinely records ionograms every 15 min; concurrent COSMIC measurements, with RO tangent points inside the square shown in Figure 1b, are selected for the analysis. The same criterion is applied for all the other ionosonde stations in selecting the COSMIC trajectories. Sometimes, it is possible that a small part of COSMIC profiles may be affected by cycle slips in the GPS phase observation data, which in some cases may result in distorted ionospheric profiles, whereas, in other cases the errors due to cycle slips may be more refined. Therefore, in selecting the data, the profile containing cycle slips resulting in distorted profile is discarded.

Ionosonde measurements provide ionospheric plasma density profile including F_2 layer peak, and the peak height is obtained from the true height inversion [Reinisch and Huang, 2001]. The Global Ionospheric Radio Observatory (GIRO) provides accurate ionospheric electron density profiles over more than 60 stations across the world. GIRO sites are equipped with Digisonde equipments that can probe bottomside ionosphere from 80 km to peak of the electron density. Real-time along with backdated data from GIRO locations are ingested in Lowell Digital Ionogram DataBase (DIDBase) and are open for public access via DIDBase web portal at <http://umlcar.uml.edu/DIDBase/>. These data are also available for public access at website of Space Physics Interactive Data Resource (<http://spidr.ngdc.noaa.gov/spidr>).

The data of ionospheric parameters (f_oF_2 , f_oF_1 , f_oE , hF_2 , hF_1 , hE , $M(3000)F_2$, etc.) are obtained from automatic ionogram scaling by Automatic Real-Time Ionogram Scaler with True height (ARTIST)-4/5, whose performance and level of error have been discussed in detail elsewhere [Reinisch et al., 2005; Mcnamara, 2006; Bamford et al., 2008; Stankov et al., 2012; Galkin et al., 2013]. Although the reliability of automatically scaled parameters by ARTIST is considerably good, some ionograms are randomly chosen for manual scaling to estimate error and to have a check. It has been observed that the magnitude of residual error for f_oF_2 and $M(3000)F_2$ arising from autoscaling varies with local time, season, and solar activity [Bamford et al., 2008; Stankov et al., 2012]. Based on statistical analysis between automatic and manual scaled data of the Dourbes (4.6°E, 50.1°N) Digisonde for the duration 2002–2008, Stankov et al. [2012] showed that the error bounds for 95% occurrence probability in each ionospheric peak parameters were f_oF_2 (−0.75, +0.85), f_oF_1 (−0.25, 0.35), f_oE (−0.35, +0.40), h_mF_2 (−68, +67), h_mF_1 (−38, +32), h_mE (−26, +2), and $M3000F_2$ (−0.55, +0.45).

For the present analysis, we have used the peak parameters (f_oF_2 and h_mF_2) downloaded from the website <http://giro.uml.edu/didbase/scaled.php>. To minimize the uncertainties arising due to autoscaling and to maintain the accuracy, we have used Confidence Score (CS) of computed data of autoscaling [Galkin et al., 2013] which is based on a system of quality criteria interspersed within the logic and algorithm of ionogram interpretation, as well as certain “sanity” checks applied to the autoscaling outcome. In the present analysis, the peak parameters (f_oF_2 and h_mF_2) for which $CS > 75$ have been considered for comparison with COSMIC data. In addition, the autoscaling technique may not be suitable for scaling the ionograms in the presence of spread F and other intense irregularities, especially in the equatorial/low-latitude regions. Spread F also affects at high latitudes. In such cases, manual scaling of ionograms is preferable. Error may also occur during manual scaling which varies from person to person. Therefore, the cases of strong spread F when autoscaling is confusing have been discarded from further analysis.

In the year 2013, the concurrent measurements during the entire year 2013 over Jicamarca (Peru) are 151 days, over Learmonth (Australia) are 253 days, over Darwin (Australia) are 219 days, over Jeju (South Korea) are 270 days, and over Juliusruh (Germany) are 350 days. The f_oF_2 and h_mF_2 data in daytime (1000–1800 LT, local time), nighttime (1800–0900 LT) [Liu et al., 2010], and for various seasons are analyzed. Both the COSMIC and ionosonde data are grouped into summer months (S) (May to August), winter months (W) (November–February), and equinox months (E) (March–April and September–October) for the Northern Hemisphere. Whereas for the Southern Hemisphere, three seasons are classified as summer months (S) (November–February), winter months (W) (May to August), and equinox months (E) (March–April and September–October).

3. Results

3.1. Jicamarca (Peru)

In order to see the departure of COSMIC-derived f_oF_2 and h_mF_2 from the ionosonde measurements, the data are considered on annual basis and then divided into day and night basis. The data are further classified into

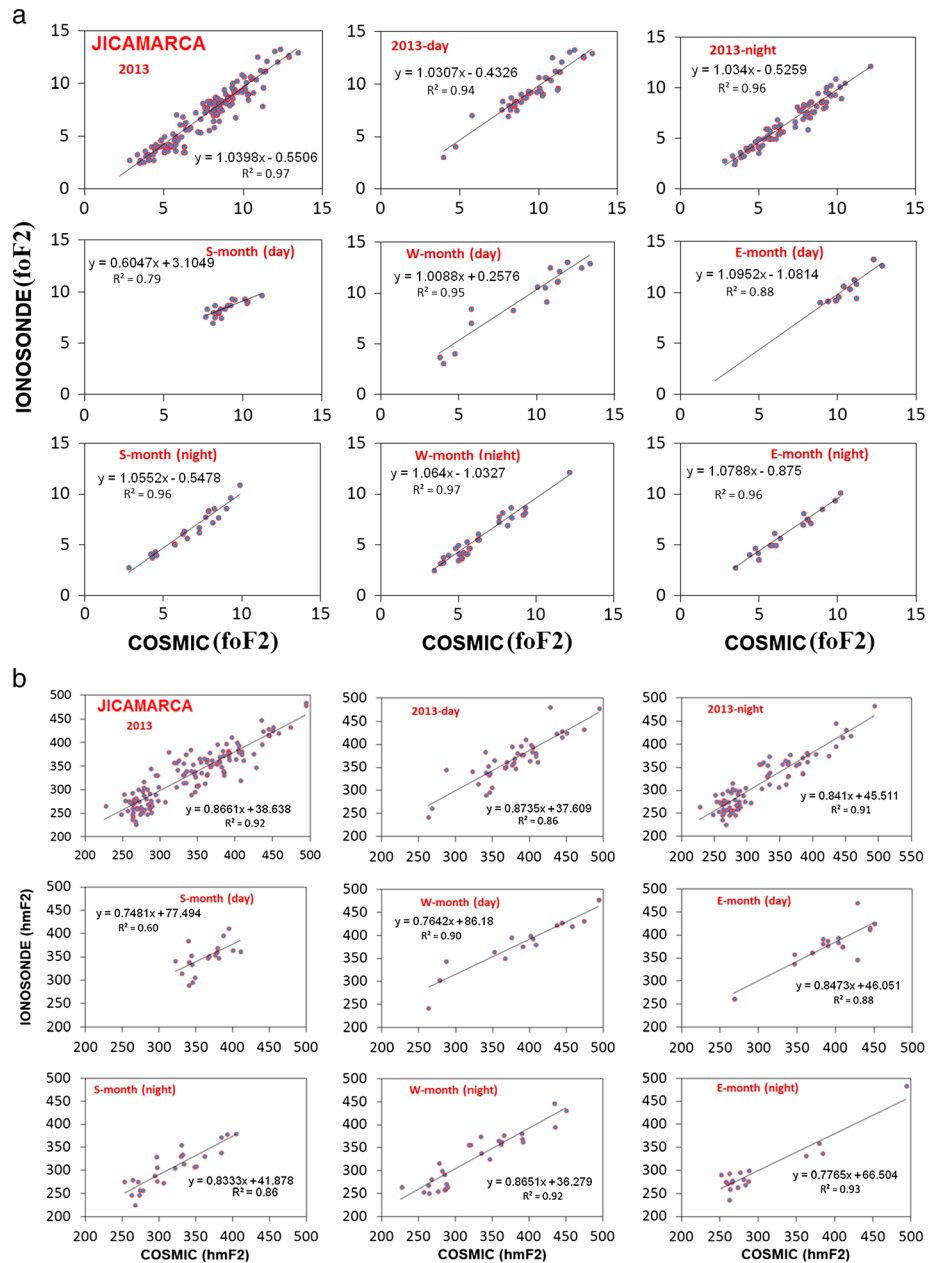


Figure 2. (a) Scattered plot and best fit linear representation of f_oF_2 estimated from COSMIC RO and ionosonde measurements at Jicamarca, Peru, for 2013, showing daytime and nighttime seasonal variations. Where S, W, and E represent summer, winter, and equinox, respectively. (b) Same as Figure 2a but for h_mF_2 .

summer, winter, and equinox months. Scattered plots and correlation diagrams for Jicamarca (Peru) are shown in Figures 2a and 2b. In addition to the autoscaled data, manual scaling has also been done to check the accuracy of autoscaled data. In this plot, data with large error (when manual scaling is confusing due to presence of spread F) have been removed from the analysis. The COSMIC-derived f_oF_2 shows almost perfect match with ionosonde data on the annual basis. The data showed relatively better correlation during the nighttime than the daytime. The day and night separation of data for different seasons shows interesting results. In the daytime of summer months f_oF_2 data are scattered only in the range 7–11 MHz. The same in nighttime is 3–10 MHz. Further, the daytime data are less correlated, and the slope of the line is less than 1 (~0.60) indicating that COSMIC is overestimating the f_oF_2 . In the nighttime slope is nearly equal to 1 (~0.91) indicating relatively better agreement with ionosonde data. In the winter and equinox months the two data sets are

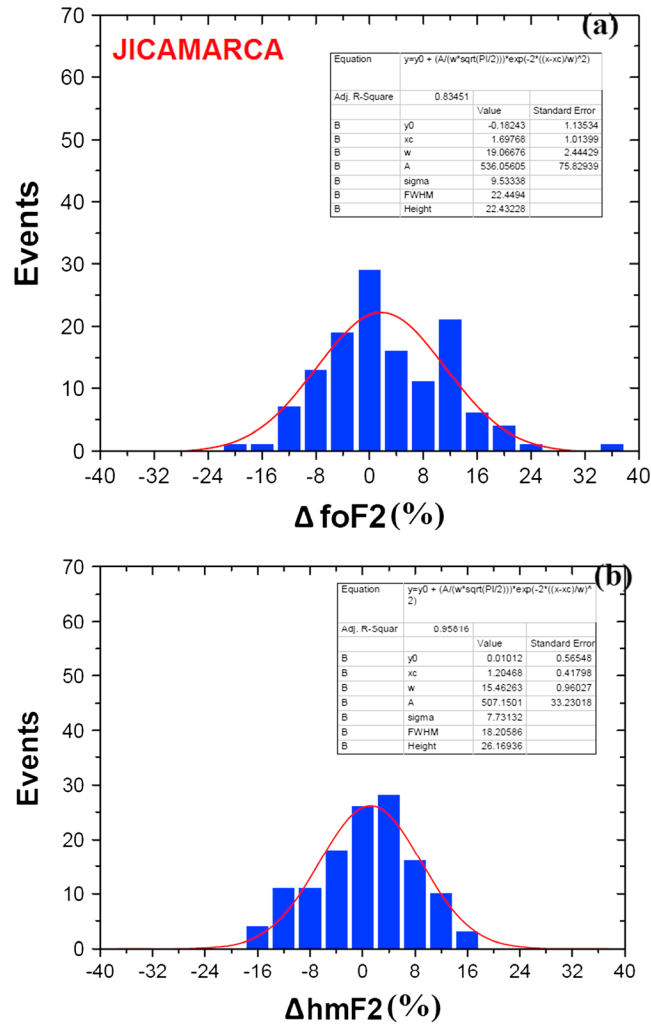


Figure 3. Histogram of occurrence of events in COSMIC RO measurements with respect to ionosonde measurement at Jicamarca, Peru, for 2013 percent error in (a) f_oF_2 and percent error in (b) h_mF_2 .

better correlated during daytime and nighttime, and also, slope in all cases lies between 1.0 and 1.06. h_mF_2 data are quite scattered as compared to f_oF_2 . There is either overestimation or underestimation of h_mF_2 in the daytime and nighttime of different seasons. For example, during daytime there is over estimation for $h_mF_2 < 350$ km or more. In the daytime for summer months, a smaller correlation is obtained. During nighttime a good correlation (with $R^2 > 0.80$) is observed in all the cases for h_mF_2 . This shows that the estimation of h_mF_2 from COSMIC profiles is quite accurate during nighttime, whereas there is large error in the daytime data. The difference between daytime and nighttime correlation coefficient for h_mF_2 is found to be the maximum during S months and the minimum during W months. E month COSMIC data show better correlation with ionosonde data during nighttime as compared to daytime data, whereas one expects relatively more error in ionosonde autoscaling due to probable presence of spread F. In nighttime high correlation may be the result of discarding of spread F-infected ionograms. Liu et al. [2010] also reported similar results over Jicamarca for the data of 2007. However, they have not mentioned about spread F.

Figures 3a and 3b show the histogram of occurrence of events in terms of percent error (Δf_oF_2 and Δh_mF_2) in COSMIC profiles at the F_2 peak altitude with respect to ionosonde measurements. The histogram has been fitted to the Gaussian function, $a_0 \exp(-z^2/2)$, where $z = (x-a_1)/a_2$ and x stands for percent error in COSMIC profile at the F_2 peak (f_oF_2), $(a_0, a_1, a_2) = (53.73, 1.68, 31.12)$. The Gaussian fitting to error occurrence yielded statistical mean error in f_oF_2 of 1.69% ($\approx 2\%$), and the full width at half maximum (FWHM) is 22.44%. Thus, the mean error is $\sim -1\%$, and the most probable error range (sigma) is $\sim \pm 13\%$. Similarly, the statistical mean error in h_mF_2 (Figure 3b) is found to be 1.20% ($\approx 1\%$), and the FWHM is 18.20%. Thus, the mean error is $\sim 1\%$, and the most probable error range (sigma) is $\sim \pm 10\%$. It is noted that there are large number of events at three and higher standard deviation from the mean. This suggests that the differences (errors) in f_oF_2 and h_mF_2 show a departure from the Gaussian distribution. This may be the result of random uncertainties in both measurements as well as observational biases.

3.2. Darwin (Australia)

Based on the scattered plots of f_oF_2 for Darwin (Australia) for the annual and daytime/nighttime of different seasons, the computed correlation coefficients are shown in Table 1. The nighttime correlation is better than the daytime. From the scatterplots (not shown) it was observed that the derived values of f_oF_2 from COSMIC measurements showed less error during nighttime than during daytime. The data were less correlated during the equinox months in daytime. The F_3/C value overestimates the ionosonde f_oF_2 value which is maximum

Table 1. Correlation Coefficient (R^2) for Different Stations and Different Seasons Are Given^a

Period	Jicamarca (Peru) 2.15°N		Darwin (Australia) 21.30°S		Jeju, (South Korea) 23.92°N		Learmonth (Australia) 31.41°S		Juliusruh (Germany) 53.96°N	
	(R^2) of f_oF_2	(R^2) of h_mF_2	(R^2) of f_oF_2	(R^2) of h_mF_2	(R^2) of f_oF_2	(R^2) of h_mF_2	(R^2) of f_oF_2	(R^2) of h_mF_2	(R^2) of f_oF_2	(R^2) of h_mF_2
2013	0.97	0.92	0.90	No Data	0.90	0.82	0.91	0.83	0.98	0.91
2013 (day)	0.94	0.86	0.80	No Data	0.66	0.75	0.48	0.82	0.94	0.84
2013 (night)	0.96	0.91	0.84	No Data	0.88	0.85	0.92	0.84	0.97	0.85
S month (day)	0.79	0.60	0.82	No Data	0.78	0.84	0.83	0.60	0.90	0.84
S month (night)	0.96	0.86	0.85	No Data	0.86	0.84	0.92	0.86	0.96	0.89
W month (day)	0.95	0.90	0.85	No Data	0.78	0.67	0.82	0.73	0.89	0.85
W month (night)	0.97	0.92	0.88	No Data	0.80	0.77	0.87	0.80	0.93	0.90
E month (day)	0.88	0.88	0.72	No Data	0.74	0.81	0.74	0.66	0.96	0.86
E month (night)	0.96	0.93	0.95	No Data	0.89	0.90	0.85	0.85	0.96	0.90

^aWhere, S, W, and E represent the summer, winter, and equinox, respectively.

during daytime of S months and minimum during daytime of W months. The h_mF_2 data for this station are not available for the year 2013. Figure 4 showed histogram of occurrence of events in terms of percent error (Δf_oF_2) in COSMIC profile. The Gaussian fitting to error occurrence yielded statistical mean error in f_oF_2 as 1.77% ($\approx 2\%$), the FWHM as 26.63%, and the most probable error range (sigma) is $\sim \pm 15\%$.

3.3. Jeju (South Korea)

The correlation coefficients for both f_oF_2 and h_mF_2 over Jeju station are given in Table 1. The f_oF_2 and h_mF_2 showed better correlation during nighttime as compared to daytime. The difference between daytime and nighttime correlations for f_oF_2 is maximum during the E months, indicating that F_3/C estimate is poorer during daytime than nighttime, with larger difference during E months. The h_mF_2 data showed higher correlation at nighttime than daytime during all the seasons except S months during which daytime and nighttime correlation coefficients are equal. Slope of the linear fit also supported that the F_3/C overestimates the ionosonde h_mF_2 with the maximum during daytime of S months and the minimum during nighttime of E months.

Figures 5a and 5b show the histogram of occurrence of events in terms of percent error for Δf_oF_2 and Δh_mF_2 , respectively. The Gaussian fitting to histogram yielded statistical mean error in f_oF_2 to be around 0.51% ($\approx 0.5\%$), and the FWHM is 18.21%, and the most probable error range is $\sim \pm 9\%$. Similarly, the statistical mean error in h_mF_2 (Figure 5b) is $\sim -1.74\%$ ($\approx -2\%$), and the FWHM is $\sim 13.92\%$ with the most probable error range $\sim \pm 7\%$.

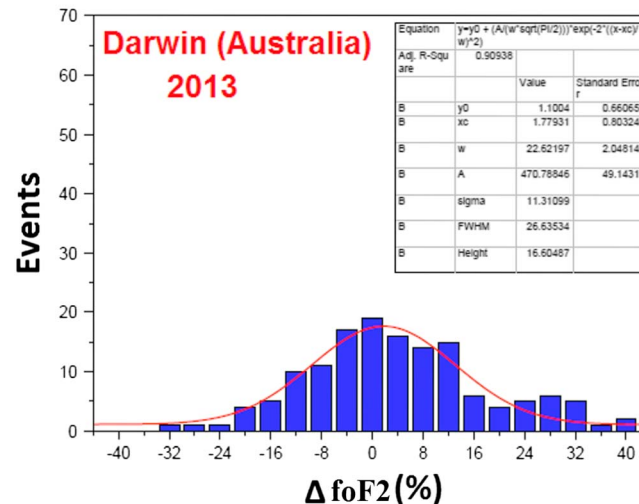


Figure 4. The same as Figure 3a but for Darwin, Australia.

3.4. Learmonth (Australia)

The correlation coefficients for f_oF_2 and h_mF_2 are given in Table 1. The data grouped in different seasons clearly depicted more scattering during daytime than in nighttime in all the seasons. The slopes of linear fit in all the cases being less than 1 indicate that the F_3/C measurements overestimate the ionosonde measurements with the maximum during daytime of equinox months. Figures 6a and 6b show the histogram of occurrence of events in terms of percent error (Δf_oF_2 and Δh_mF_2) in COSMIC profile. The statistical mean error in f_oF_2 is $\sim 0.70\%$ ($\approx 1\%$), the full width at half maximum is $\sim 18.16\%$, and the most probable error range is $\sim \pm 9\%$. Similarly,

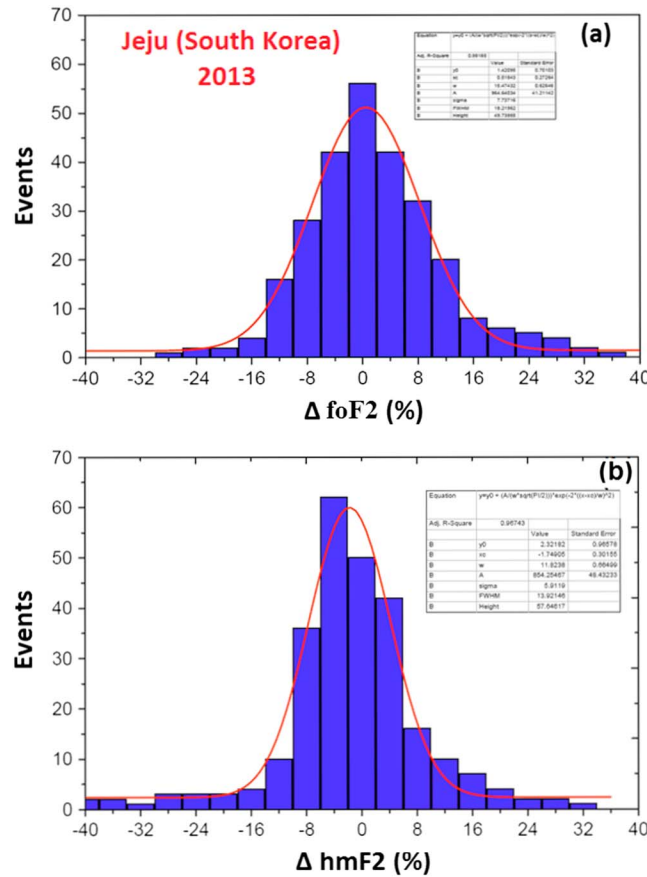


Figure 5. The same as Figure 3 but for Jeju, South Korea, percent error in (a) f_oF_2 and percent error in (b) h_mF_2 .

tudes. Further, at this station the difference in daytime and nighttime correlation is found to be maximum during S months and minimum during E months. Comparison among the data of this station indicates relatively larger departure during S months. The Gaussian fitting to percent error (Δf_oF_2 and Δh_mF_2) (Figures 7a and 7b) occurrences yielded statistical mean error in f_oF_2 of $\sim -1\%$ ($\approx -1\%$), and the full width at half maximum as $\sim 15.97\%$ and the most probable error range (sigma) is $\sim \pm 8\%$. Similarly, the statistical mean error in h_mF_2 (Figure 7b) is $\sim -2.32\%$ ($\approx -2\%$), the FWHM is $\sim 12.43\%$, and the most probable error range is $\sim \pm 6\%$.

3.6. Space Weather Impact on the Accuracy of COSMIC Profiles

For this study, we have considered three cases of geomagnetic storms which occurred on 1–5 May 2013, 1–5 June 2013, and 17–20 March 2015. The *Dst* index variations describing the intensity and duration of geomagnetic storms are shown in Figures 8a–8c. The considered geomagnetic storms are of different intensity with *Dst* varying between -65 nT and -225 nT. The development and decay time scales of considered storms are different. An intense storm is expected to produce larger perturbations in the atmosphere, which may be different at different locations. During these geomagnetic storms periods, COSMIC measurements over the stations Jicamarca (Peru), Jeju (South Korea), and Learmonth (Australia) are available which are analyzed. The altitude profiles of plasma frequency for the COSMIC and ionosonde measurements over Jicamarca (Peru) during the geomagnetic storm of 1 June 2013 at around 1506 h LT are shown in Figure 9a. For a comparison the plasma frequency profile during quite day on 12 June 2013 at around the same time is shown in Figure 9a. For this station no data are available for the storm of May 2013. There is large difference between the two profiles near the F_2 peak and above in the case of storm as compared to quiet period. However, there is no difference below 300 km altitude both during the quiet and storm period. The difference (error) in COSMIC f_oF_2 from the ionosonde during the quiet day of 12 June 2013 was 0.8 MHz ($\sim 10\%$) which became 1.5 MHz ($\sim 19.25\%$) during the geomagnetic storm period. The difference in h_mF_2 is also found to be larger during the storm day (134 km, 50%) as compared to quiet day (-17 km, 5%).

the statistical mean error in h_mF_2 (Figure 6b) is $\sim 1.76\%$ ($\approx -2\%$), and the FWHM is $\sim 13.71\%$. From the Gaussian fitting the most probable error range (sigma) is $\sim \pm 7\%$.

3.5. Juliusruh (Germany)

Based on the scattered plots (not shown) correlation coefficients are determined and are given in Table 1. Interestingly, f_oF_2 plots on the annual basis (not given), day and night cases, and even in different seasons show good correlation with the correlation coefficient lying between 0.85 and 0.99. h_mF_2 data show scattered distribution as compared to f_oF_2 data. There is underestimation of COSMIC-derived h_mF_2 especially during night hours of winter months as well as in the annual data. The correlation coefficient for h_mF_2 lies between 0.85 and 0.90. The correlation coefficient for day and night during all the seasons for both data sets f_oF_2 and h_mF_2 is found to be quite close to each other as compared to the equatorial and low-latitude stations. This shows that the COSMIC measurements are much more reliable at midlatitudes as compared to the equatorial and low lati-

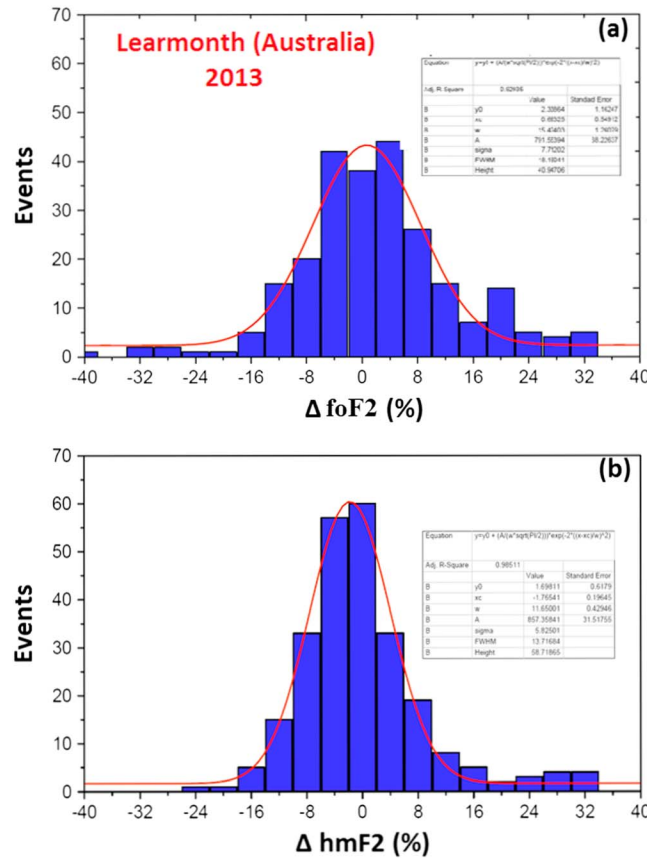


Figure 6. The same as Figure 3 but for Learmonth, Australia, percent error in (a) f_oF_2 and percent error in (b) h_mF_2 .

measurements, whereas the same is over estimated above the F_2 peak. The difference is larger during the geomagnetic storm period as compared to the quiet period. COSMIC satellite did not pass over Jeju region during the storm period of 1 June 2013.

The corresponding profiles over Learmonth, Australia, for both the storms and quiet days are given in Figures 9c and 9d. The discrepancy in f_oF_2 for the May 2013 storm was 0.64 MHz (13%) and during the quiet period was ~ 0.18 MHz (4%). The error in h_mF_2 during the storm period was 17 km, 4.5%, and the quiet period was -2 km, 0.6%. For the storm of June 2013 the difference in f_oF_2 during the storm period is 2.73 MHz ($\sim 31\%$) which is also larger than that of quiet period value (0.44 MHz, $\sim 6\%$). The difference in h_mF_2 during the storm period was 5 km (8.6%) larger than that during the quiet period (-4 km, 6%). During the quiet days in the month of May 2013, below F_2 peak, COSMIC measurements show quite close value to the ionosonde value. However, above the F_2 peak some deviation in the two measurements is observed. During the storm period, the deviation between COSMIC and ionosonde enhances above F_2 peak as compared to the quiet period.

For the geomagnetic storms of 17 March 2015, COSMIC and ionosonde measurements over the station Jeju (South Korea) are only available. The corresponding profiles for the storm day (17 March) and quiet day (22 March) are shown in Figure 8d. The discrepancy in f_oF_2 for the storm day was found to be 4.03 MHz (43%), and during quiet day it was ~ 0.85 MHz (9%). The error in h_mF_2 during the storm period was -17 km, 5%, and the quiet period was -7 km, 2.5%. An increase in the intensity of geomagnetic storm showed enhanced error in f_oF_2 and decreased error value in h_mF_2 . However, because of the limited number of events analyzed, no conclusion can be derived on the role of the intensity of storm.

3.7. Discussion

The results of correlation analysis of f_oF_2 and h_mF_2 during daytime and nighttime for both annual and seasonal (summer, winter, and equinox) variations are summarized in Table 1. The correlation coefficient (R^2) varies

The large difference between COSMIC and ionosonde data above F_2 peak may also be due to incorrect estimation of ionosonde data because of ionogram scaling by considering the same scale height at F_2 peak and above. During disturbed condition this may cause large error in ionosonde data. Thus, the difference includes errors introduced in observational technique as well as error introduced in ionogram scaling of ionosonde.

Similarly, plasma frequency profiles over Jeju (South Korea) during the geomagnetic storm of 1 May 2013 (Figure 9b) showed that the difference between the two profiles became significantly enlarged during the geomagnetic storm period as compared to the quiet period. The difference in f_oF_2 during the quiet day of May 2013 was 0.5 MHz ($\sim 4\%$) which became 2.34 MHz ($\sim 20\%$) during the storm period. The difference in peak height (Δh_mF_2) was also larger during the geomagnetic storm period (23 km, 7.5%) than during the quiet period (19 km, 6.5%). Further, electron density (plasma frequency) below the F_2 peak is underestimated by COSMIC

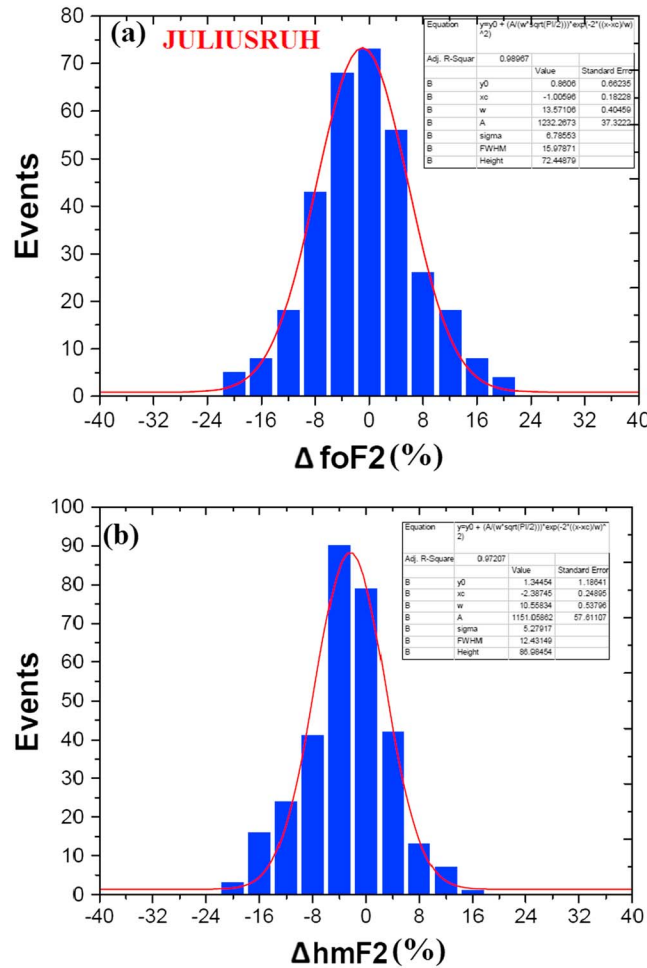


Figure 7. The same as Figure 3 but for Juliusruh, Germany, percent error in (a) f_oF_2 and percent error in (b) h_mF_2 .

electron density gradients. A northward wind configuration could transport plasma toward higher altitudes along geomagnetic field lines in the Southern Hemisphere and to lower altitudes in the Northern Hemisphere. Consequently, the recombination rates would be higher/lower in the Northern/Southern Hemisphere. Furthermore, *Batista et al.* [2011] showed that the density response to changes in height due to meridional wind is very fast and could also contribute to the observed discrepancies. Thus, the electron density in the north could be lower than in the south. A change in the orientation of the wind may change the response in N_mF_2 and h_mF_2 .

In the present analysis the largest error (difference) in COSMIC RO-derived f_oF_2 is from the low-latitude station Darwin (Australia), located in the EIA region. The enhanced error may possibly be due to the existence of large electron density gradient, a prominent feature of this region, which is ignored by the spherically symmetric assumption used in Abel inversion [*Tsai et al.*, 2001; *Tsai and Tsai*, 2004; *Liu et al.*, 2010; *Ely et al.*, 2012; *Kumar et al.*, 2014]. Large density gradient may be present during sunrise/sunset of local hours, geomagnetic storms, and near EIA regions particularly during high solar activity year [*Jakowski et al.*, 2002]. Contrary to our results (overestimation of f_oF_2 both during the daytime and nighttime above certain altitude), *Liu et al.* [2010] showed that electron density profiles generally underestimate during the nighttime and overestimate during the daytime. The overestimation is below the F_2 peak. They also reported significant errors at lower altitudes at the equatorial and low latitudes. We also found that the errors of over estimation of f_oF_2 were largest in the summer months both during the daytime and nighttime. During the summer months the equatorial ionization anomaly in association with wind pattern may create significant density gradient leading to large error in the estimation of electron density profiles. Further, in Abel inversion, significant error appears below the F_2 peak

between 0.60 and 0.98. An increase with latitude is suggestive of less error (difference) in the profiles of COSMIC-derived f_oF_2 and h_mF_2 data at midlatitudes. This is also supported by the error analysis of the data. In general, f_oF_2 data have better correlation (Table 1) than h_mF_2 data, with a maximum difference at the equatorial station Jicamarca (Peru). For this region *Ely et al.* [2012] also reported better correlation for N_mF_2 as compared to h_mF_2 and also reported that the peak height measured by satellite to be lower than the height provided by Digisonde. On the annual basis, our analysis showed this trend up to altitudes ~ 330 km, whereas at higher altitudes satellite-measured values are, in general, higher than ionosonde data. Around the same latitude range, *Chu et al.* [2010] reported correlation coefficient (R^2) of 0.86 for N_mF_2 from November 2006 to February 2007 for the quiet period ($K_p < 3$). *Ely et al.* [2012] argued that the difference in position and local time are not sufficient parameter to account for the observed discrepancies. They further suggested that these differences could be attributed to the local conditions such as the presence of transequatorial wind or

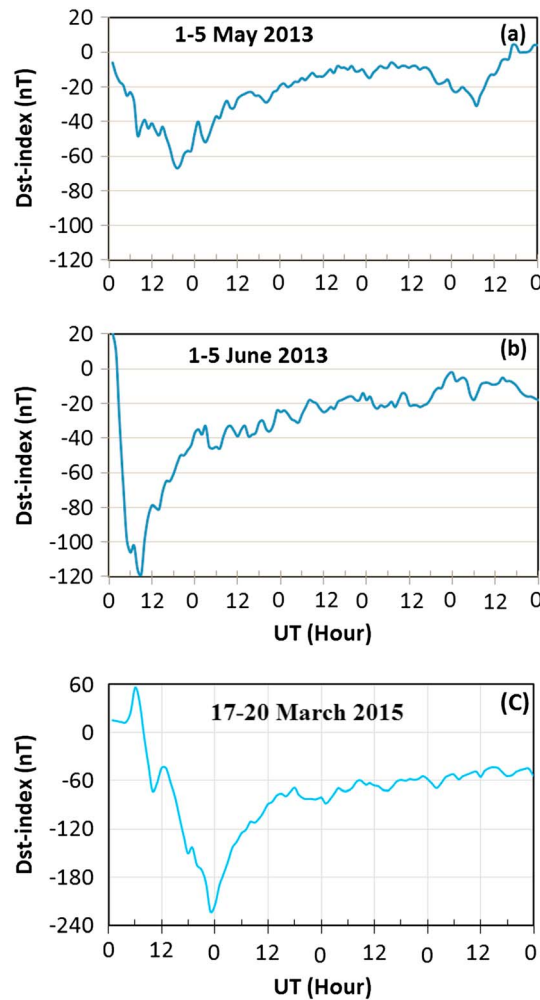


Figure 8. Variation of *Dst* index showing occurrence of geomagnetic storms (a) during 1–5 May 2013, (b) during 1–5 June 2013, and (c) during 17–20 March 2015.

(standard deviation) values. Figure 10 shows the percentage of events having Δf_oF_2 and Δh_mF_2 lying between 2σ and 3σ , 3σ and 4σ , and $> 4\sigma$ for different stations. Due to the presence of large number of events in the tail region, the same can be categorized as fat tailed distribution. The fat tail distributions are more evident during summer and equinox seasons. The formation of fat tail distribution is significantly observed for f_oF_2 over Jicamarca, Darwin, and Juliusruh, whereas the same for h_mF_2 are observed over Jicamarca and Juliusruh. A large number of events at three or more standard deviations above the mean value of error may not necessarily be from random uncertainties in the ionosonde and COSMIC measurements. A large number of events with high sigma values occurring over the equatorial station Jicamarca may be the result of the presence of spread *F* in the ionograms which could lead to misinterpretation of the data in addition to other factors. Further, the asymmetry in the horizontal distribution of the electron density around the ionosonde stations may also lead to large error, which is ignored while deriving the electron density profile from COSMIC measurements using Abel inversion. In the analysis of COSMIC signal, the Snell's law of refraction is replaced by the Bouger's law which usually leads to overestimation in the electron density. Apart from the instrumental limitations, the difference (error) may also depend on how the signals observed in the two instruments interact with the ionosphere structure. The ionosonde uses radio frequencies (5–15 MHz) and works on the principle of reflection when signal frequency becomes equal to the plasma frequency of the ionospheric layer. Snell's law of reflection/refraction is used, and the effect of collisions and magnetic fields is neglected. The wavelength being of the order of tens of meters is affected by the irregularities of larger size. In the case of COSMIC, frequency used is 1575 MHz

layer as compared to above the peak [Schreiner *et al.*, 1999; Yue *et al.*, 2010]. As a result COSMIC measurements could be more realistic as compared to ionosonde data above the F_2 peak. The recovery of profile from ionosonde measurements assumes the same scale height at F_2 peak and above, which may not be true.

The daytime correlation coefficient is smaller than the nighttime correlation, with a maximum difference at EIA region during the equinox months. As compared to the equatorial and low-latitude regions, the difference of daytime and nighttime correlation at midlatitudes is found to be relatively smaller. A summary of error analysis is given in Table 2. The mean error in f_oF_2 is about 1% (except at Darwin where it is $\sim 2\%$) with most probable range 15% in the equatorial and low-latitude region, which decreases with increase in latitude and becomes 7% at Juliusruh. The mean error in h_mF_2 is $\sim 5\%$ in the equatorial region and decreases to $\sim 2\%$ at midlatitudes. The most probable error in h_mF_2 decreases from 10% (near the equator) to 7% at higher ($>23^\circ$) latitudes. The Gaussian distribution of Δf_oF_2 and Δh_mF_2 at almost all the stations shows the presence of large number of observations at three or more σ

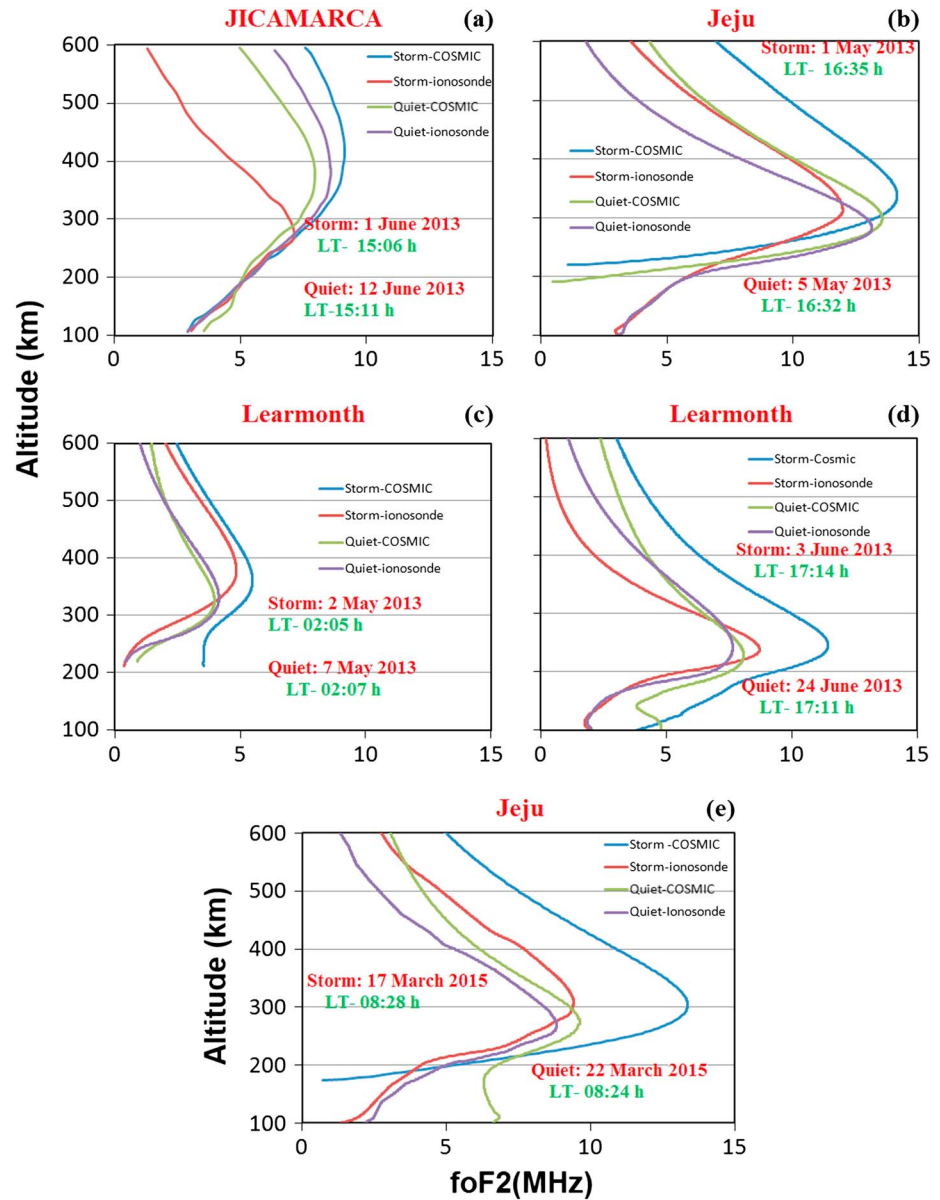


Figure 9. Comparison of COSMIC RO plasma frequency profile with ionosonde at (a) Jicamarca, Peru, during geomagnetic storm day of 1 June 2013 and quiet day of 12 June 2013, (b) Jeju, South Korea, during geomagnetic storm of 1 May 2013 and quiet of 5 May 2013, (c) Learmonth, Australia, during geomagnetic storm day of 2 May 2013 and quiet day of 7 May 2013, (d) Learmonth, Australia, geomagnetic storm of 3 June 2013 and during quiet day of 24 June 2013. (e) Jeju, South Korea, during storm of 17 March 2015 and quiet day 22 March 2015.

Table 2. Mean Error and Most Probable Range in Percent for f_oF_2 and h_mF_2 at Different Stations Are Given

Error	Jicamarca (Peru) 2.15°N	Darwin (Australia) 21.30°S	Jeju (South Korea) 23.92°N	Learmonth (Australia) 31.41°S	Juliusruh (Germany) 53.96°N
Mean error in f_oF_2	-1.7%	2%	0.5%	1%	-1%
Most probable range (sigma) for f_oF_2	±13%	±15%	±9%	±9%	±8%
Mean error in h_mF_2	1%	NA	-2%	-2%	-2%
Most probable range (sigma) for h_mF_2	±10%	NA	±7%	±7%	±6%

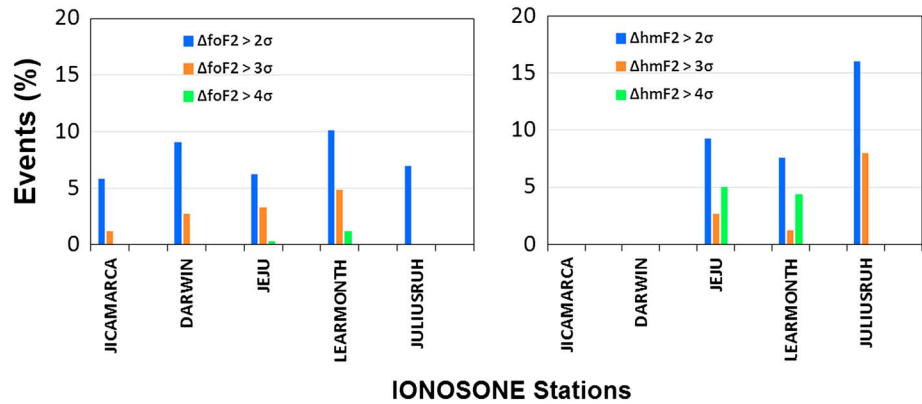


Figure 10. The percentage distribution of events having Δf_oF_2 and Δh_mF_2 lying between 2σ and 3σ , 3σ and 4σ , and $> 4\sigma$ for different stations.

(L_1 signal) and 1275 MHz (L_2 signal) and corresponding wavelengths are 19 cm and 24 cm. These signals can be affected by very small size irregularities (few meters to 100 m). Thus, large scale irregularities have little effect on COSMIC signals. The small-scale irregularities cause diffractive scintillations in the propagating signals. As a result amplitude/phase of the signal is modified [Kintner et al., 2007].

At the equatorial regions, during the daytime the steepest gradients, sharp peaks and deep valleys, and density crests occur due to the fountain effect on both sides of the equator forming equatorial ionization anomaly [Appleton, 1946; Martyn, 1955; Kumar and Singh, 2009] which may result in larger latitudinal density gradient leading to larger error in COSMIC RO during the daytime as compared to nighttime. However, these phenomena are insignificant over midlatitude regions, and as a result there may not be significant difference between daytime and nighttime correlations as observed. The daytime electron density gradient in the ionosphere is largest during the equinoctial months (E months) at equatorial and low latitudes because of the EIA development. Liu et al. [2010] found that during the daytime at Jicamarca, where EIA is well-developed F_3/C overestimates N_mF_2 otherwise generally F_3/C underestimated both N_mF_2 and h_mF_2 .

Space weather users are usually interested in the altitudinal electron density profile and its variability during quiet and disturbed conditions. Comparing the plasma frequency (electron density) profiles during three geomagnetic storms and quiet times at three stations, it is observed that storm time difference (errors) is larger than those during the quiet periods, with the maximum difference observed for the storm of 17 March 2015, which was the most intense considered storm. The trend shows that there is larger-scale variability of the equatorial ionosphere during geomagnetic storm periods as compared to midlatitude. This may be because of the geomagnetic field geometry, which in collaboration with the disturbed daytime electric field could produce larger electron density gradients [Lin et al., 2005; Fejer et al., 2007; Siingh et al., 2005, 2007, 2015; Singh et al., 2011; Kumar and Singh, 2011a, 2011b; Kumar et al., 2012]. As a result of enhancement in storm intensity, the impact of storm increases, and consequently, error is amplified.

The electron density profile above F_2 peak cannot be directly measured by ionosonde, and hence, it is extrapolated assuming constant ionosphere-scale height (equal to the scale height at F_2 peak). This causes error in electron density (plasma frequency) profile. This error varies with local time and ionospheric disturbances [Reinisch et al., 2001]. The accuracy of electron density profile depends on the correlations of the scaling of ionograms, and different softwares developed have some assumptions which may lead to error [Huang and Reinisch, 1996; Reinisch and Huang, 1983; Reinisch et al., 2005; Galkin et al., 2013]. Thus, above F_2 peak, ionosonde data are not the exact ones; hence, the difference (error) in COSMIC and ionosonde data may include error in ionosonde profile as well as error in Abel inversion of COSMIC data, which is amplified during the disturbed conditions. The ionogram scaling above F_2 peak during the disturbed condition is a real problem, and much more effort is needed in this direction especially during disturbed conditions when scale height is variable and very ill defined. In order to establish a relation between errors introduced in electron density profiles, N_mF_2 and h_mF_2 and intensity of storms and its variability with latitudes more data analysis during different geomagnetic storms and solar flares at different stations are required.

4. Conclusion

The plasma frequency profiles derived from COSMIC and ionosonde measurements are analyzed at five stations covering wide latitude range from the equator to midlatitudes in both the Northern and Southern Hemisphere. Based on the analysis, following points emerged:

1. The f_oF_2 and h_mF_2 derived from COSMIC RO measurements are compared with the ground-based ionosonde measurements. The correlation coefficient (R^2) for f_oF_2 and h_mF_2 has been computed by grouping the data in day and night in different seasons. The nighttime data showed better correlation implying that the two data sets are close to each other. The lowest correlation represents the largest error, which occurred during the equinox months. These errors could not be attributed to the position and local time differences between the satellite measurement position and the ground-based stations. Therefore, these errors may be attributed to the presence of electron density gradient which increases during the daytime and further enhances during the equinox months.
2. The Gaussian fitting to errors showed the maximum probable error ($\sim \pm 15\%$) at the equatorial and EIA stations, which reduced to $\pm 8\%$ at midlatitude stations. This is in accordance with the fact that the latitudinal density gradient decreases with increase in latitude, and hence, errors introduced to the Abel's inversion during the estimation of electron density also decrease with latitude. The errors as well as FWHM at low-latitude stations are larger than that of midlatitudes. These errors may be both due to random uncertainties in measuring techniques/instruments and probing signal interaction with the ionospheric plasma. The latter one may arise because of difference in wavelengths of the two signals.
3. Error in COSMIC RO measurements increases during geomagnetic storms, which further enhances with the intensity of storm. Results are explained considering electric fields (prompt penetration and disturbance dynamo electric field) which strengthen density gradients through $E \times B$ instability mechanism. However, it is not known whether the role of electric field in creating error is linear or nonlinear. Further study is required to resolve this issue. In any study of space weather event involving ionospheric electron density profile, we need to use the profile containing the geomagnetic storm time element as well as quiet time element. The estimated magnitude of error during storm time hints the programmer to make suitable corrections. The present study gives a direction for such corrections.

Acknowledgments

The authors would like to express their gratitude to the University Corporation for Atmospheric Research (UCAR) and the National Space Organization (NSPO) in Taiwan for making available the FORMOSAT-3/COSMIC constellation data (<http://cdaac-www.cosmic.ucar.edu>). We are thankful to Global Ionospheric Radio Observatory (GIRO) and GIRO Principal Investigator B. W. Reinisch of the University of Massachusetts Lowell for making the data files available and Maintenance team for SAO Explorer to provide ID and password of LGDC Account. Indian Institute of Tropical Meteorology, Pune, is funded by Ministry of Earth Sciences (MoES). The data used in this paper are available with Sanjay Kumar and Devendraa Siingh (e-mail; sanjay.skitvns@gmail.com; devendraa-siingh@gmail.com). The SERB, New Delhi, is cordially acknowledged for providing assistance under Young Scientist Scheme (project SR/FTP/ES-164/2014). The authors wish to thank the Editor and anonymous reviewers for their critical comments and valuable suggestion, which helped to improve the paper.

References

- Appleton, E. V. (1946), Two anomalies in ionosphere, *Nature*, *157*, 691–693.
- Aragon-Angel, A., Y.-A. Liou, C.-C. Lee, B. W. Reinisch, M. Hernández-Pajares, M. Juan, and J. Sanz (2011), Improvement of retrieved FORMOSAT-3/COSMIC electron densities validated by ionospheric sounder measurements at Jicamarca, *Radio Sci.*, *46*, RS5001, doi:10.1029/2010RS004578.
- Bamford, R. A., R. Stamper, and L. R. Cander (2008), A comparison between the hourly autoscaled and manually scaled characteristics from the Chilton ionosonde from 1996 to 2004, *Radio Sci.*, *43*, RS1001, doi:10.1029/2005RS003401.
- Batista, I. S., E. M. Diogo, M. A. Abdu, and G. J. Bailey (2011), Equatorial ionization anomaly: The role of thermospheric winds and the effects of the geomagnetic field secular variation, *Aeronomy Earth's Atmos. Ionosphere*, *2*, 317–328, doi:10.1007/978-94-007-0326-1_23.
- Cheng, C. Z., Y. H. Kuo, R. A. Anthes, and L. Wu (2006), Satellite constellation monitors global and space weather, *Eos Trans. AGU*, *87*, 166.
- Chu, Y.-H., K.-H. Wu, and C.-L. Su (2009), A new aspect of ionospheric E region electron density morphology, *J. Geophys. Res.*, *114*, A12314, doi:10.1029/2008JA014022.
- Chu, Y.-H., C.-L. Su, and H.-T. Ko (2010), A global survey of COSMIC ionospheric peak electron density and its height: A comparison with ground-based ionosonde measurements, *Adv. Space Res.*, *46*, 431–439, doi:10.1016/j.asr.2009.10.014.
- Chuo, Y.-J., C.-C. Lee, W.-S. Chen, and B. W. Reinisch (2013), Comparison of the characteristics of ionospheric parameters obtained from FORMOSAT-3 and Digisonde over Ascension Island, *Ann. Geophys.*, *31*, 787–794, doi:10.5194/angeo-31-787-2013.
- Ely, C. V., I. S. Batista, and M. A. Abdu (2012), Radio occultation electron density profiles from the FORMOSAT-3/COSMIC satellites over the Brazilian region: A comparison with Digisonde data, *Adv. Space Res.*, *49*, 1553–1562.
- Fejer, B. G., J. W. Jensen, T. Kikuchi, M. A. Abdu, and J. L. Chau (2007), Equatorial ionospheric electric fields during the November 2004 magnetic storm, *J. Geophys. Res.*, *112*, A10304, doi:10.1029/2007JA012376.
- Galkin, I. A., B. W. Reinisch, X. Huang, and G. M. Khmyrov (2013), Confidence score of ARTIST-5 ionogram autoscaling, INAG Tech. Memorandum page 1–7, November 25, 2013.
- Ghodpage, R. N., D. Siingh, R. P. Singh, G. K. Mukherjee, P. Vohat, and A. K. Singh (2012), Tidal and gravity waves study from the airglow measurements at Kolhapur (India), *J. Earth Syst. Sci.*, *121*, 1511–1525.
- Hajj, G. A., and L. J. Romans (1998), Ionospheric electron density profiles obtained with the global positioning system: Results from the GPS/MET experiment, *Radio Sci.*, *33*, 175–190, doi:10.1029/97RS03183.
- He, M., L. Liu, W. Wan, B. Ning, B. Zhao, J. Wen, X. Yue, and H. Le (2009), A study of the Weddell Sea Anomaly observed by FORMOSAT-3/COSMIC, *J. Geophys. Res.*, *114*, A12309, doi:10.1029/2009JA014175.
- Hu, L., B. Ning, L. Liu, B. Zhao, Y. Chen, and G. Li (2014), Comparison between ionospheric peak parameters retrieved from COSMIC measurement and ionosonde observation over Sanya, *Adv. Space Res.*, *54*, 929–938, doi:10.1016/j.asr.2014.05.012.
- Huang, X., and B. W. Reinisch (1996), Vertical electron density profile from Digisonde ionograms. The average representative profile, *Ann. Geophys.*, *39*(4), 756–757.

- Jakowski, N., A. Wehrenpfennig, S. Heise, C. Reigber, H. Lühr, L. Grunwaldt, and T. K. Meehan (2002), GPS radio occultation measurements of the ionosphere from CHAMP: Early results, *Geophys. Res. Lett.*, *29*(10), 1457, doi:10.1029/2001GL014364.
- Kelley, M. C., V. K. Wong, N. Aponte, C. Coker, A. J. Mannucci, and A. Komjathy (2009), Comparison of COSMIC occultation-based electron density profiles and TIP observation with Arecibo incoherent scatter radar data, *Radio Sci.*, *44*, RS4011, doi:10.1029/2008RS004087.
- Kintner, P. M., B. M. Ledvina, and E. R. de Paula (2007), GPS and ionospheric scintillations, *Space Weather*, *5*, S09003, doi:10.1029/2006SW000260.
- Kirchengast, G., U. Foelsche, and A. Steiner (Eds.) (2004), *Occultations for Probing Atmosphere and Climate*, Springer-Verlag, Berlin, Heidelberg, isbn:978-3-540-22350-4.
- Krankowski, A., I. Zakharenkova, A. Krypiak-Gregorczyk, I. I. Shagimuratov, and P. Wielgosz (2011), Ionospheric electron density observed by FORMOSAT-3/COSMIC over the European region and validated by ionosonde data, *J. Geod.*, doi:10.1007/s00190-011-0481-z.
- Kumar, S., and A. K. Singh (2009), Variation of ionospheric total electron content in Indian low latitude region of equatorial ionization anomaly (EIA), *Adv. Space Res.*, *43*, 1555–1562.
- Kumar, S., and A. K. Singh (2011a), Storm time response of GPS-derived total electron content (TEC) during low solar active period at Indian low latitude station Varanasi, *Astrophys Space Sci.*, *331*, 447–458.
- Kumar, S., and A. K. Singh (2011b), GPS derived ionospheric TEC response to geomagnetic storm on 24 August 2005 at Indian low latitude stations, *Adv. Space Res.*, *47*, 710–717.
- Kumar, S., S. Priyadarshi, G. K. Seemala, and A. K. Singh (2012), GPS-TEC variations during low solar activity period (2007–2009) at Indian low latitude stations, *J. Astrophys. Space Sci.*, *339*, 165–178.
- Kumar, S., E. L. Tan, S. G. Razul, C. M. S. See, and D. Siingh (2014), Validation of IRI-2012 model with GPS based ground observation over low-latitude Singapore station, *Earth, Planet and Space*, *66*, 1–10.
- Kuo, Y.-H., T.-K. Wee, S. Sokolovskij, C. Rocken, W. Schreiner, D. Hunt, and R. A. Anthes (2004), Inversion and error estimation of GPS radio occultation data, *J. Meteorol. Soc. Japan*, *82*(1B), 507–531.
- Lei, J., et al. (2007), Comparison of COSMIC ionospheric measurements with ground-based observations and model predictions: Preliminary results, *J. Geophys. Res.*, *112*, A07308, doi:10.1029/2006JA012240.
- Lin, C. H., A. D. Richmond, R. A. Hellis, G. J. Bailey, G. Lu, J. Y. Liu, H. C. Yeh, and S.-Y. Su (2005), Theoretical study of the low- and midlatitude ionospheric electron density enhancement during the October 2003 superstorm: Relative importance of the neutral wind and the electric field, *J. Geophys. Res.*, *110*, A12312, doi:10.1029/2005JA011304.
- Liou, Y. A., A. G. Pavelyev, S. S. Matyugov, O. I. Yakovlev, and J. Wickert (2010), in *Radio Occultation Method for Remote Sensing of the Atmosphere and Ionosphere*, edited by Y. A. Liou, pp. 170, InTech, Vokovar, Croatia, isbn:978-953-7619-60-2.
- Liu, L., B. Zhao, W. Wan, B. Ning, M.-L. Zhang, and M. He (2009), Seasonal variations of the ionospheric electron densities retrieved from Constellation Observing System for Meteorology, Ionosphere, and Climate radio occultation measurements, *J. Geophys. Res.*, *114*, A02302, doi:10.1029/2008JA013819.
- Liu, L., W. Wan, B. Ning, M.-L. Zhang, M. He, and X. Yue (2010), Longitudinal behaviors of the IRI-B parameters of the equatorial electron density profiles retrieved from FORMOSAT-3/COSMIC radio occultation measurements, *Adv. Space Res.*, *46*, 1064–1069.
- Liu, L., H. Le, Y. Chen, M. He, W. Wan, and X. Yue (2011), Features of the middle- and low-latitude ionosphere during solar minimum as revealed from COSMIC radio occultation measurements, *J. Geophys. Res.*, *116*, A09307, doi:10.1029/2011JA016691.
- Martyn, D. F. (1955), *The Physics of the Ionosphere* (London: The Physical Society), p. 260.
- McNamara, L. F. (2006), Quality figures and error bars for autoscaled Digisonde vertical incidence ionograms, *Radio Sci.*, *41*, RS4011, doi:10.1029/2005RS003440.
- Parkinson, B. W., and J. J. Spilker Jr. (1996), *Global Positioning System: Theory and Applications*, vol. 1 and 2, pp. 485–496, Am. Inst. Aeronautics, 370 L'Enfant Promenade, SW, Washington, DC.
- Reinisch, B. W., and X. Huang (1983), Automatic calculation of electron density profiles from digital ionograms: 3. Processing of bottom side ionograms, *Radio Sci.*, *3*, 477–492, doi:10.1029/RS018i003p00477.
- Reinisch, B. W., and X. Huang (2001), Deducing topside profiles and total electron content from bottomside ionograms, *Adv. Space Res.*, *27*(1), 23–30.
- Reinisch, B. W., X. Huang, A. Belehazi, and R. Ilma (2001), Using scale heights derived from bottom side ionograms for modeling the IRI topside profile, *Adv. Radio Sci.*, *2*, 293–297.
- Reinisch, B. W., X. Huang, I. A. Galkin, V. Paznukhov, and A. Kozlov (2005), Recent advances in real-time analysis of ionograms and ionospheric drift measurements with digisondes, *J. Atmos. Solar Terr. Phys.*, *67*(12), 1054–1062.
- Rocken, C., Y.-H. Kuo, W. Schreiner, D. Hunt, S. Sokolovskiy, and C. McCormick (2000), COSMIC system description, *Terr. Atmos. Ocean Sci.*, *11*, 21–52.
- Schreiner, W. S., S. V. Sokolovski, C. Rocken, and D. C. Hunt (1999), Analysis and validation of GPS/MET radio occultation data in the ionosphere, *Radio Sci.*, *34*, 949–966, doi:10.1029/1999RS900034.
- Siingh, D., R. P. Singh, A. K. Kamra, P. N. Gupta, R. Singh, V. Gopalakrishnan, and A. K. Singh (2005), Review of electromagnetic coupling between the Earth's atmosphere and the space environment, *J. Atmos. Sol. Terr. Phys.*, *67*, 637–658, doi:10.1016/j.jastp.2004.09.
- Siingh, D., V. Gopalakrishnan, R. P. Singh, A. K. Kamra, S. Singh, V. Pant, R. Singh, and A. K. Singh (2007), The atmospheric global electric circuit: An overview, *Atmos. Res.*, *84*, 91–110.
- Siingh, D., R. P. Singh, S. Kumar, T. Dharmaraj, A. K. Singh, A. K. Singh, M. N. Patil, and S. Singh (2015), Lightning and middle atmospheric discharges in the atmosphere, *J. Atmos. Sol. Terr. Phys.*, *134*, 78–110.
- Singh, A. K., D. Siingh, and R. P. Singh (2011), Space weather: Physics, effects and predictability, *Sur. Geophys.*, *31*, 581–638.
- Stankov, S. M., J.-C. Jodogne, I. Kutiev, K. Stegen, and R. Warnant (2012), Evaluation of automatic ionogram scaling for use in real-time ionospheric density profile specification: Dourbes DGS-256/ARTIST-4 performance, *Ann. Geophys.*, *55*(2), doi:10.4401/ag-4976.
- Straus, P. R. (2007), Ionospheric climatology derived from GPS occultation observations made by the ionospheric occultation experiment, *Adv. Space Res.*, *39*, 793–802.
- Syndergaard, S., W. S. Schreiner, C. Rocken, D. C. Hunt, and K. F. Dymond (2006), Preparing for COSMIC: inversion and analysis of ionospheric data products, in *Atmosphere and climate: studies by occultation methods*, edited by U. Foelsche, G. Kirchengast, and A. K. Steiner, pp. 137–146, Springer, New York.
- Tsai, L. C., and W. H. Tsai (2004), Improvement of GPS/MET ionospheric profiling and validation using the Chung-Li IONOSONDE measurements and the IRI model, *Terr. Atmos. Ocean Sci.*, *15*, 589–607.
- Tsai, L. C., W. H. Tsai, W. S. Schreiner, F. T. Berkey, and J. Y. Liu (2001), Comparisons of GPS/MET retrieved ionospheric electron density and ground based ionosonde data, *Earth Planets Space*, *53*, 193–205.
- Tsai, L. C., C. H. Liu, and T. Y. Hsiao (2009), Profiling of ionospheric electron density based on the FormoSat/3 COSMIC data: Results from the intense observation period experiment, *Terr. Atmos. Oceanic Sci.*, *20*, 181–191, doi:10.3319/TAO.2007.12.19.01(F3C).

- Wu, X., X. Hu, X. Gong, X. Zhang, and X. Wang (2009), An asymmetry correction method for ionospheric radio occultation, *J. Geophys. Res.*, *114*, A03304, doi:10.1029/2008JA013025.
- Yue, X., W. S. Schreiner, J. Lei, S. V. Sokolovskiy, C. Rocken, D. C. Hunt, and Y.-H. Kuo (2010), Error analysis of Abel retrieved electron density profiles from radio occultation measurements, *Ann. Geophys.*, *28*, 217–222, doi:10.5194/angeo-28-217-2010.
- Yue, X., et al. (2012), Global 3-D ionospheric electron density reanalysis based on multisource data assimilation, *J. Geophys. Res.*, *117*, A09325, doi:10.1029/2012JA017968.
- Yue, X., W. S. Schreiner, N. Pedatella, R. A. Anthes, A. J. Mannucci, P. R. Straus, and J.-Y. Liu (2014), Space weather observations by GNSS radio occultation: From FORMOSAT-3/COSMIC to FORMOSAT-7/COSMIC-2, *Space Weather*, *12*, 616–621, doi:10.1002/2014SW001133.
- Zakharenkova, I., A. Krankowski, I. Shagimuratov, Y. V. Cherniak, A. Krypiak-Gregorczyk, P. Wielgosz, and A. F. Lagovsky (2012), Observation of the ionospheric storm of October 11, 2008 using FORMOSAT-3/COSMIC data, *Earth Planets Space*, *64*, 505–512.